Front. Struct. Civ. Eng. 2025, 19(4): 524–540
https://doi.org/10.1007/s11709-025-1177-4

RESEARCH ARTICLE

Integrated ground penetrating radar and deep learning approach for rebar diameter classification in concrete elements

Mostafa KHEDR[a], Mahmoud METAWIE[b], Mohamed MARZOUK[b*]

[a] *Integrated Engineering Design Management Program, Faculty of Engineering, Cairo University, Giza 12613, Egypt*
[b] *Structural Engineering Department, Faculty of Engineering, Cairo University, Giza 12613, Egypt*
[*] *Corresponding author. E-mail: mmarzouk@cu.edu.eg*

ABSTRACT Traditional evaluation of reinforced rebar in concrete elements involves destructive methods that may harm the building. This paper introduces a framework that adopts non-destructive techniques to classify rebar in reinforced concrete elements. The framework integrates Ground Penetrating Radar (GPR) with deep learning to automate rebar detection and analysis in concrete elements. The framework consists of four stages: Data sets Creation, Data sets Processing, Steel Rebar Detection Model, and Transfer Learning. Different deep learning models are tested to choose the highest-performing model. The YOLO v8 model outperforms Faster R-CNN and YOLO v7. The selected YOLO v8 model is trained on experimental and site data and then tested on real data from the building to validate the model's accuracy and ability to classify rebar diameter. Integrating GPR with deep learning can potentially improve the accuracy and efficiency of rebar detection in structural assessments.

KEYWORDS reinforced concrete inspection, non-destructive testing, GPR, rebar diameter classification, deep learning, YOLO v8

1 Introduction

Inspecting and evaluating the quality of reinforced concrete is crucial in civil and infrastructure engineering. Due to the potential risks associated with structural failure [1]. One of the most critical factors to validate is rebar. Accurate identification and description of reinforcing rebars in a concrete structure is essential for ensuring construction quality control and evaluating safety measures for buildings at various stages of the project [2]. Furthermore, examining the diameters of rebar and the spacing between them is vital for fabricators and site engineers to ensure that the dimensions align with the design model during the manufacturing and construction phases. The bearing capacity of reinforced concrete structures is determined by the dimensions and position of the rebar [2]. Additionally, the presence of cracks in concrete surfaces can impact the effectiveness of reinforcement repairs, potentially leading to corrosion and a reduction in the bond between materials [3]. These cracks can also increase the exposed surface area, causing more stress and further reducing the durability and strength of the structure [4]. Cracks in concrete not only affect durability but also compromise long-term structural performance. Cracks have a detrimental effect on concrete structures due to their impact on the accuracy of load-bearing capacity assessments and overall safety. Additionally, the cost of repairs and maintenance can be significant, making early detection and assessment crucial for ensuring long-term structural health and cost-effectiveness [5]. Therefore, it is crucial to closely monitor the condition of concrete surfaces and address any cracks quickly to maintain the structure's integrity. Repairing cracks is essential to prevent further damage and maintain structural integrity. Various methods for modeling cracks help determine the most effective repair technique [6].

Commonly utilized methods for detecting rebar are

Article history: Received Nov 28, 2024; Accepted Jan 21, 2025

considered destructive, such as coring, which can compromise the integrity of the structure. Several factors have been found to influence the measured accuracy, including the length or diameter ratio of the core, the diameter of the core, and the direction of drilling [7].

Ground penetrating radar (GPR) is considered one of the important non-destructive techniques (NDT) methods in construction. It can be used to inspect reinforcement rebar within concrete, identify underground utilities, and evaluate the structural integrity of buildings [8]. GPR is commonly used for detecting reinforcement rebar and voids in concrete structures, providing valuable information for restoration projects. This technology allows for a more thorough assessment of the building's condition without causing any damage to the structure. GPR operates by emitting and receiving electromagnetic waves. The electromagnetic reflections from diverse objects such as steel reinforcement bars, cavities, or other materials exhibit hyperbolic or linear configurations with varying polarization and signal strength. Through detailed examination of these reflections, it leads to determine the object case [9]. However, the interpretation of GPR data requires specialized training and expertise to accurately identify potential issues. To address this challenge, artificial intelligence (AI) can be utilized to streamline the process and provide more accurate results. The visual interpretation of GPR data by a skilled professional requires a significant amount of time and effort. The process of interpreting GPR data takes a lot of time, and possibly even longer, to be fully completed. Therefore, it affects the effectiveness of decision-making for maintenance and repair purposes [10]. Utilizing AI can help streamline the process and improve accuracy by reducing human error and providing more efficient analysis of large data sets [11]. Additionally, AI algorithms can quickly identify patterns and trends in data that may not be immediately apparent to human analysts. By incorporating AI and deep learning into non-destructive testing analysis, the potential for human error in interpreting data can be minimized, ultimately leading to more efficient and effective interpretation [12]. The integration of GPR data with machine learning algorithms is crucial for obtaining high-quality data sets and addressing challenges caused by factors that affect GPR waves, such as environmental influences and the time-consuming process of data interpretation. This requires the combination of both signal processing and image processing techniques. Advanced deep learning frameworks and automated systems exhibit high accuracy and efficiency, pushing the boundaries of GPR applications in construction. This progress paves the way for various applications, including underground utility detection and structural health monitoring. Additionally, these technologies enable real-time data analysis, as well as the detection and classification of rebar diameter and corrosion assessment in rebar.

This research presents a framework that integrates deep learning techniques and GPR images for the localization and classification of diameter in reinforced concrete slabs and columns of rebar. By combining the capabilities of deep learning with the imaging provided by GPR, the framework improves accuracy and efficiency in detecting and analyzing rebar in concrete structures. It developed an automated method to convert GPR source files into images for data set creation, utilizing a Python script. The research enhances the precision and efficiency of GPR hyperbola detection and localization by implementing the classification using the You Only Look Once version 8 (YOLO v8), a deep learning object detection model that processes an image only once to provide bounding box coordinates and probabilities for objects of interest [13]. The model incorporates a new backbone network as its fundamental architecture, which allows for faster detection and higher accuracy [14]. The proposed method is evaluated and validated using data set of different samples of different diameters of steel rebar, capturing actual conditions of finishing materials such as sand, granite, and ceramic. The developed system can be integrated into existing building detection processes, facilitating time and cost efficiency in construction projects by reducing the need for manual inspection and verification of rebar placement and diameter. These tasks are often labor-intensive, time-consuming, and require skilled workers. Additionally, the system provides real-time feedback and can be integrated with several non-destructive methods for assessing the quality of concrete structures. This ensures that any issues are promptly identified and addressed to prevent potential structural failures in the future.

2 Literature review

The pursuit of NDT in construction has become increasingly important in recent years. NDT techniques include ultrasonic testing, thermography, ground-penetrating radar, and eddy current testing [15]. Using NDT in construction offers several benefits; it allows for the early detection of structural issues [16], it provides a more accurate assessment of structural integrity, and the use of NDT can extend the lifespan of structures by identifying and addressing problems before they worsen over time [17]. Additionally, the utilization of NDT for concrete enables comprehensive monitoring by assessing, analyzing, and forecasting physical degradation mechanisms and performance attributes [18].

2.1 Factors affecting ground penetrating radar signals

GPR is a popular non-destructive testing method for identifying hidden objects due to its high efficiency,

acceptable resolution, and easy portability [19]. The GPR device utilizes electromagnetic wave technology and consists of three essential components: first, the Antenna System, which transmits and receives electromagnetic waves into the ground; second, the Signal Processing Unit, which analyzes the received signals to generate subsurface images; and third, the Control/Display Unit, a computer device that allows the user to interact with the GPR system. This unit provides a user-friendly interface for controlling the GPR system and visualizing the collected data [15]. GPR uses a transmitting antenna to send electromagnetic waves toward a targeted area. The speed of these waves changes based on the electrical and magnetic characteristics of the materials encountered. Some of the energy is reflected back to the surface due to these changes. Additionally, the interactions between different materials within a composite significantly influence how the waves behave as they pass through, affecting the way energy is reflected and scattered [20]. After the receiving antenna records the reflected data, it is transmitted to a processing unit. This processing unit analyzes the data and applies algorithms to produce visual results. These visual results provide a representation of the underground structures or materials encountered by the GPR [21]. GPR signals are affected by a combination of technical, physical, and environmental factors, making it challenging to accurately interpret and analyze the data. First, technical factors effected by GPR brand and model, coupling method, frequency, and polarization. Second, physical factors such as rebar diameter and configuration, surface, and overlayers. Third, environmental factors such as moisture, chloride, and corrosion by products [15]. Pressure and temperature are among the factors affecting the reinforcing steel rebars, and they impact the structural integrity and durability of reinforced concrete. GPR can be effective in detecting subsurface anomalies in concrete and analyzing their effects on the rebar [22]. Accurate interpretation and analysis of GPR signals require a comprehensive understanding of these factors. Each factor plays a crucial role in influencing the quality and reliability of the data obtained from GPR surveys.

For instance, a sample of these factors was considered while designing a controlled environment on specimens, which was then followed by testing on real case studies to validate the findings of the framework. According to a study by Zhou et al. [2], rebar diameter and cover thickness in concrete structures affect the GPR wave. The study conducted experiments to investigate this relationship. The results demonstrate a direct correlation between decreasing rebar diameter and normalized GPR amplitude values. Furthermore, these results show that GPR can be a reliable, non-destructive testing method for accurately predicting rebar diameters and estimating cover thickness in both laboratory and field settings. Different surfaces, like air, asphalt, concrete, rebar, or the bottom of a slab, reflect energy waves in different ways because their physical properties can change the signals that are received by GPR [23]. In addition to that, cracks, delamination, or surface coatings, can cause variations in the reflection and scattering of energy waves, leading to changes in the GPR signal patterns. The impact of cracks varies according to their size. Tesic et al. [24] found that cracks up to 0.9 mm did not have much of an effect on the loss of electromagnetic energy and did not make a big difference in the GPR signal attenuation. In addition to that, Hong et al. [25] found that the decrease in rebar diameter and increase in corrosion induced crack width resulted in a reduction in the amplitude of the reflected wave. Additionally, the corrosion development caused a decrease of approximately 2.0 in amplitude and an increase of approximately 1.5 in the travel time of the reflected wave. This indicates that the amplitude and arrival time increase with the increasing height of the corrosion product filling. Therefore, checking the crack sizes is crucial for accurately assessing the rebar diameter.

Cracks in concrete have the potential to enhance the entry of moisture and chloride, which will consequently change the relative conductivity and permittivity of the concrete, which will have an impact on the attenuation of radar signals [26]. Lachowicz and Rucka [27] find that the presence of a large amount of water in the concrete led to a notable reduction in the velocity of radar waves, affecting the detection and assessment of potential issues. These findings emphasize the importance of considering moisture content when interpreting GPR results for concrete structures.

2.2 Reinforcing bars identification

Integrating automated solutions into rebar recognition can improve efficiency and reduce manual labor. Detecting rebar in GPR pictures is challenging due to limited contrast, low signal-to-noise ratio, and field data complexity [28]. Kaur et al. [29] introduced a framework for automated identification and examination of reinforcing bars based on an autonomous bridge inspection system equipped with a GPR sensor. The approach utilizes a combination of machine learning categorization, image-based gradient characteristics, and precise curve fitting to analyze the hyperbolic signature of rebar. The final result of comparing the framework's rebar region detector to a number of image-based classification algorithms shows that the proposed framework is precise at detection. Moreover, it was tested on real bridge decks. Ahmed et al. [30] introduced a multistage deep encoder-decoder network for detecting rebar in concrete bridge deck. The model was trained on an image data set on a per-pixel basis, where pixels representing rebars are assigned as objective labels, while

all other pixels are assigned as insignificant labels. The study examined many architectures for the deep network and concluded that the most effective one combined the SegNet-MobileNet encoder with the ResNet-Xception encoder module. Xiong and Tan [31] utilized a comparison between different YOLO models, based on deep learning techniques, to analyze the tie bars in GPR images. The compared models are YOLO-V4-tiny, YOLO v3, YOLO-v3-tiny, and YOLO-V4. The researchers considered 2185 waves reflected from tie bars that are distributed across 670 GPR images in the GPR image data set, which is divided into training and validation sets. The results demonstrate that YOLO-V4 achieves higher levels of accuracy, recall, F1-score, and mean average precision (mAP) that corresponds to 99.2%, 99.6%, 99.4%, and 99.74%, respectively.

2.3 Automated classification of reinforcing bars

Measuring the radius of reinforcement rebar is considered an essential step in ensuring the structural integrity and safety of concrete structures. Various methodologies are employed including theoretical, physical modeling and utilizing machine learning. Chang et al. [32] proposed a method for identifying the diameter of rebar utilizing digital image processing techniques. The framework depends on the quality of the reflected signal obtained from GPR. The results of this study demonstrated that this method can accurately estimate the radius, with an error margin of only 7% compared to the actual size. Furthermore, the methodology was validated in a controlled environment rather than in an actual case study, indicating that the model must be tested before being applied in field work. Giannakis et al. [33] developed a machine-learning framework that is capable of precisely determining the diameter of the rebar under investigation, utilizing the resolution range of the antenna. The proposed methodology integrates neural networks and random forest regression and has been entirely trained using synthetic data and then tested via actual data. Moreover, the creation of synthetic data, which involves data simulation, plays a crucial role, particularly when real-world data collection is limited. By training models on simulated data from the beginning, it can lead to better predictive performance [34]. Xiang et al. [35] introduced a method for determining the depth and dimensions of rebar in GPR data. First, the hyperbola signal in the GPR data are detected by the processes of eliminating the direct wave, reconstructing the signal, and separating it. A database is established by utilizing a collection of theoretical hyperbolas, which are subsequently compared to the extracted outlines of hyperbolas. The rebar depth and size are determined by finding the closest match in the database. The results demonstrated that the utilized method can effectively eliminate the direct wave disturbance by the GPR data and accurately extract the outlines from the interlaced hyperbolas. To solve the problem of setting rules for the classification of the massive size of the data and its label using deep learning, it is important to find the rule and compare the data and its label. Deep learning algorithms effectively learn and characterize input data, then make predictions or decisions based on that learning. This process allows the algorithm to continually improve its performance and accuracy over time [36]. These models have the ability to generalize well and extract complex patterns and features from the data, making them highly effective in solving classification problems. Additionally, deep learning algorithms can continuously learn and improve their classification accuracy over time as more data are fed into the system. Liu et al. [37] introduced an automated framework for detecting and identifying rebar using deep learning and migration techniques. This framework applies a time-zero correction filter for GPR images. To remove the time delay between the transmission and reception of the GPR signal. This ensures that the data are aligned, and the hyperbolas are correctly detected. Then, the trained Single Shot Detector (SSD) model is employed to detect hyperbolas in the GPR image and identify specific regions of interest (RoI). The test results demonstrate that the suggested system has a detection accuracy of 90.9%. Park et al. [38] introduced a framework that utilizes the YOLO v3 model for detecting rebar diameter. The model was trained on experimental data, consisting of an acrylic box specimen with dimensions of 80 cm × 80 cm× 50 cm and holes. Each hole had a diameter of 31 mm and was positioned at a height of 25 cm to enter the rebar inside it. The training results demonstrated a decline in the loss curves of both B-scan and migrated data, suggesting that both data sets were effectively learned without experiencing overfitting. The model's performance improved over time as the number of training rounds increased, indicating its capacity to acquire knowledge.

3 Research methodology

GPR data interpretation requires specialized training and expertise to accurately identify potential issues due to errors in target recognition and poor signal-to-noise ratio, in addition to surrounding environmental effects [39]. The proposed framework provides an approach to integrating automated methods for creating the data and the most recent and commonly used deep learning model, YOLO v8, for object detection due to its efficiency in object detection tasks and its performance in real-time applications [40]. By automating the task, the framework aims to enhance the accuracy and efficiency of GPR image analysis tasks. The utilized methodology consists

of four main stages: 1) data sets creation, 2) data processing, 3) steel rebar detection model, and 4) model evaluation. Figure 1 illustrates the relationships among framework stages along with their designated outputs.

3.1 Data sets creation

Generating an accurate data set is a key component of successfully training AI models. A well-defined and balanced data set provides the model with the necessary information for training, leading to improved generalization and more consistent performance in real-world applications, which directly impacts the model's ability to make accurate predictions across various scenarios [41]. These improvements significantly enhance the model's overall effectiveness and its ability to deliver accurate predictions across diverse situations. It is important to note that the GPR signal is affected by various factors, including the thickness of the concrete layer, the size of the reinforcing bar, and the electrical properties of the concrete surrounding the bar, such as relative permittivity and dielectric constant [32]. The data set simulates the environment that is close to the real case and incorporates factors such as rebar diameter, rebar case, and concrete content. In the designed specimens, the embedded rebars are placed in locations commonly found in real-world structures [9]. The simulated environment allows the model to learn how these variables affect the GPR wave patterns. Furthermore, the use of simulated data, followed by integration with real-world data, enhances detection efficiency, conserves resources, and enables the model to be applied to a wider range of scenarios and conditions due to its ability to adapt and learn from diverse data sources [42].

The designed data set consists of three groups.

1) Group 1 consists of three simple wooden boxes with dimensions of 1 m × 0.3 m × 0.3 m. Each box contains embedded reinforced rebars of one diameter size (Ø16, Ø18, and Ø20) as depicted in Fig. 2(a).

2) Group 2 consists of wooden boxes with dimensions of 1 m × 1 m × 0.6 m, and the box contains seven embedded pipes, which allows for easier modification and customization of the rebar inside it that increases the level of complexity and trains the model in a wider range

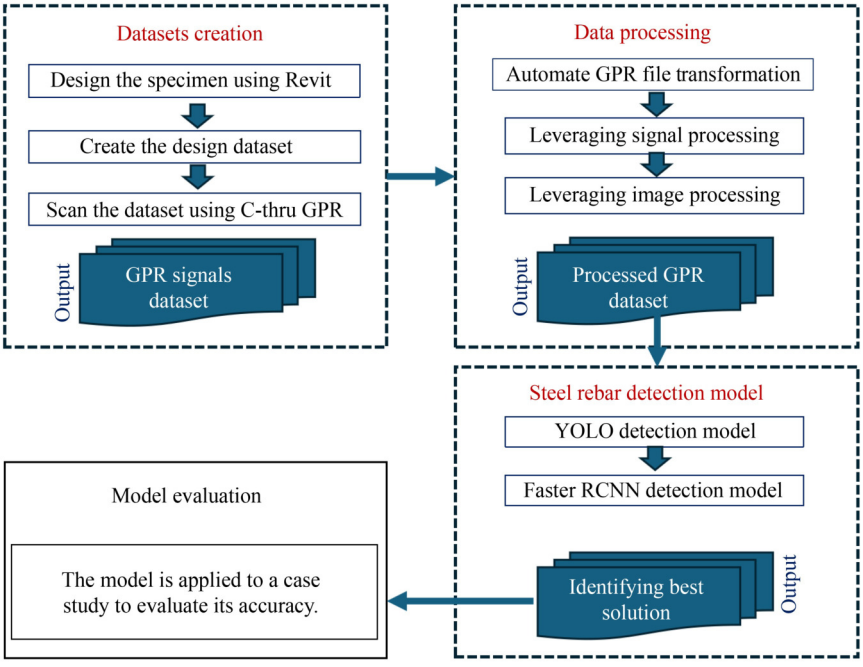

Fig. 1 Proposed framework methodology.

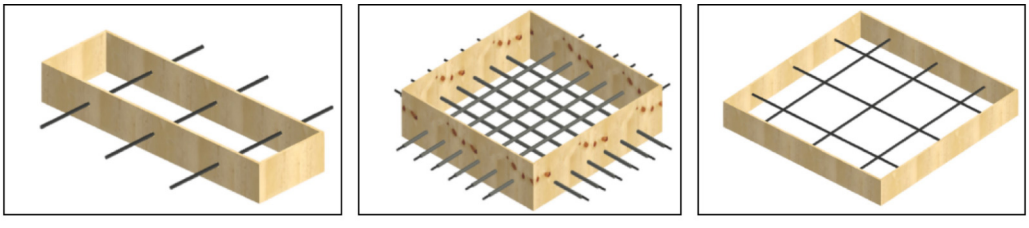

Fig. 2 3D Models of designated specimens: (a) group 1; (b) group 2; (c) group 3.

of cases. The length and width were increased to simulate the case of a slab containing two layers of reinforcement, upper and lower reinforcement. Moreover, it provides more space for scanning and tracking the change of the GPR wave at different spots. The utilized diameter sizes are Ø12, Ø18, and Ø20 (Fig. 2(b)).

3) Group 3 consists of three wooden boxes with dimensions of 0.6 m × 0.6 m × 0.3 m. Each box contains three embedded reinforced rebars in two directions: horizontal and vertical. The main reason for this design is to validate the previous two groups and ensure that the pipes in the second group do not have any effect on the rebar. The same diameter sizes as in the second group are used (Fig. 2(c)).

The fabrication of the three groups of specimens involved accurately measuring and cutting the wooden boxes to the specified dimensions. Once the boxes were assembled, the reinforced rebars or pipes were carefully embedded in both horizontal and vertical directions within each box. Concrete was poured into each box to fill it completely. The specimens were left for curing before being scanned with GPR. Figure 3 shows the three created groups, which are categorized as the first group, the second group, and the third group. The C-thru handle GPR device was used to scan the specimens. It was calibrated for each group before scanning. Each group was scanned in different positions. Different types of finishing above surfaces were added to the second group, such as granite, sand, and ceramic, to examine their effect on the rebar diameter because of the size of the specimen, which allowed for multiple variations in the collected data set.

3.2 Training artificial intelligence model procedures

Training an AI model involves a sequence of organized processes designed to help the algorithm learn and apply patterns from data [43]. Each step is crucial in ensuring the model's accuracy and efficiency, from data preprocessing to model evaluation. The quality of the training data and the chosen hyperparameters can greatly impact the final performance of the AI model [44]. Moreover, the choice of algorithm and the size of the training data set also play a significant role in determining the success of the AI model which consists of five main phases: data preprocessing, feature engineering, model evaluation, algorithm selection, and transfer learning. It is important to continuously iterate and fine-tune these components to achieve optimal results. Figure 4 demonstrates the procedures for training the AI model. An important aspect of the machine learning process is data preprocessing. The first phase, data processing, involves data cleaning, transforming, and preparation. Data cleaning involves removing any irrelevant or duplicate images, handling missing values, and correcting inconsistencies to ensure the quality of the data set. Additionally. Data sampling for training ensures that the entire data are represented to avoid bias modeling. Proper data preparation is crucial for accurate model training and reliable results in machine learning applications. This step helps ensure that the algorithm can effectively learn from the data and make accurate predictions.

Feature engineering is another crucial phase in the machine-learning process. It involves selecting the most relevant data features to improve the model's performance [45]. Common techniques used with GPR data include image processing and signal processing techniques. Image processing techniques can be used to extract important features from images, such as texture, shape, color, and highlighting the target object within the image. Signal processing techniques can be used to filter noise, enhance the signal-to-noise ratio, and extract meaningful patterns from the data. Another important aspect of feature engineering is dimensionality reduction, which involves reducing the number of features in a data set while retaining as much relevant information as possible. Data augmentation is also a key component of feature engineering. It involves generating new data samples from suitable existing data to improve the model' s generalization capabilities [46]. The data can be manipulated by implementing a range of transformations, such as cropping, rotating, and flipping. By generating new data images through these techniques, the model can become more robust and accurate in its predictions. This process can help prevent overfitting and improve the model's performance on unseen data.

The algorithm selection phase plays a key role in determining the success of a machine learning project. Evaluating and comparing multiple algorithms can help

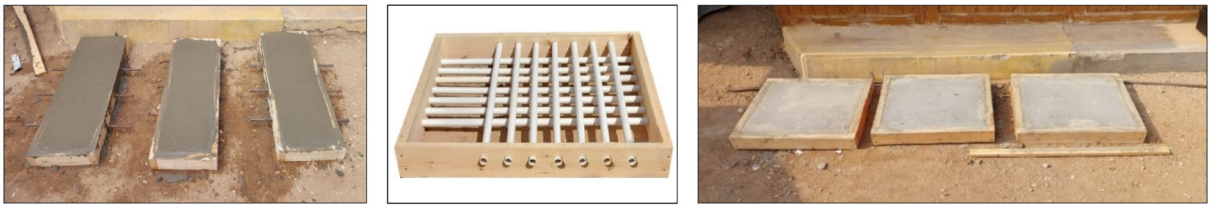

(a) (b) (c)

Fig. 3 Fabricated specimens groups: (a) group 1; (b) group 2; (c) group 3.

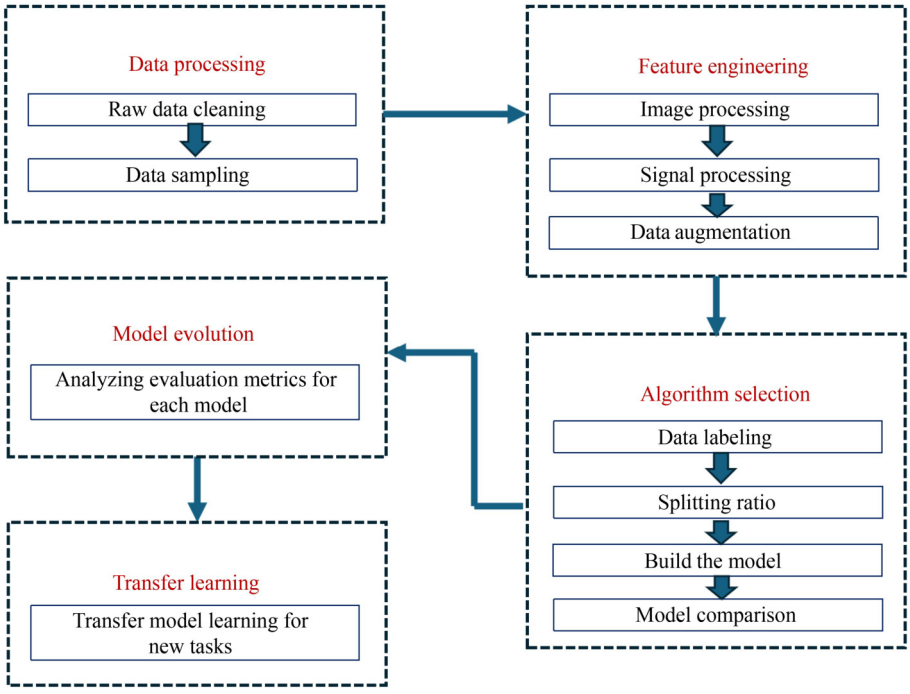

Fig. 4 Training AI model procedure.

achieve the best possible results. In addition to choosing the right algorithm, the size and quality of the training data set are also important factors to consider [47]. Splitting the data into appropriate percentages is important. Commonly used methods, such as train-test split or cross-validation, can help ensure that the model generalizes well to unseen data. Hyperparameters are another critical component in machine learning, as they determine how a model learns from the training data [47]. Train-test split is a common technique where the data set is divided into two subsets for training and testing the model [48]. These methods help evaluate the ability to generalize new data and make accurate predictions. The model evaluation phase involves analyzing evaluation metrics, adjusting various components, and updating the model with changes in the data or environment. The phase helps ensure the model remains relevant and reliable in various scenarios. After training the model and obtaining satisfactory results, the model can be saved and used. Transfer Learning phase is a powerful technique that allows the knowledge gained from training one model to be applied to another task, saving time and resources [49]. This approach can help improve the performance of new models by leveraging the insights and patterns learned from previous training processes.

3.3 Data processing

3.3.1 Automate ground penetrating radar data transformation

Converting GPR signals into images is a crucial step in analyzing GPR data. By visualizing the signals as images it allows for easier interpretation, comparison, and accessibility of GPR data set [50]. The developed script utilizes libraries from both the Python and R languages to automate the image creation process. These libraries include rpy2 [51] which enables seamless integration between Python and R, NumPy [52] which is considered a fundamental library for numerical computing in Python that provides efficient operations and array manipulation, matplotlib [53] that is used for data visualization.

The code is developed to carry out a number of actions using designated functions. The first function, Data Reading function, aims to convert raw GPR data into a more usable and structured format for further analysis and visualization. The second function, Data Plotting function, plots the data to convert the representative numbers into pixels for an image. The third function, Data Decoding function, begins by entering the main input file path and velocity as inputs. It then sets the global environment for the file path and the source code for the R code, which is stored in the variable r_source. Next, the function utilizes the R language to extract other data, such as traces, position, and depth. Finally, the function checks the velocity. If provided, the function uses it; if not, the function sets a default value. The output is then used in the subsequent stages of data processing. The Data decoding function aims to convert raw GPR data into a more usable and structured format for further analysis or visualization. It acts as an accumulation function that leverages the functionality of the previous two functions: data plotting and data reading functions. The function operates by iterating through each given

directory, reading the raw data using the reading data function, and creating a data frame by combining the data. The output of the scripted code is compared to the output from the Reflexw GPR processing software by entering the data without any modifications and comparing the resulting images. Figure 5 illustrates this comparison, showing images generated by both the Python code and Reflexw software. It mainly highlights the differences in visualization techniques. However, the number of hyperbolas is equal in both images, which indicates the efficiency of the code.

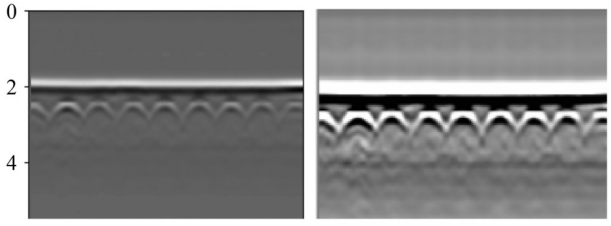

Fig. 5 Validation GPR data transformation: (a) image generated by Python code; (b) image generated by Reflexw.

3.3.2 Leveraging signal processing

To enhance the quality of low-resolution data, signal processing techniques are being utilized, which offer different advantages to facilitate result interpretation [54]. The applied approach consists of three main filtering steps: first, applying a high-pass filter that allows only high-frequency components to pass through while removing all pixels below a specified range [55]. Second, applying a median filter, which is used to replace each pixel with the median value of its neighboring points, makes it effective at preserving signal features while reducing noise [56]. Third, apply the dewbow filter, which eliminates the low-frequency vibrations generated by electromagnetic induction and corrects low-frequency and direct current bias in the data [57]. Figure 6 shows the final results after applying the signal processing system. For GPR scanning, the third group consists of a specimen of a wooden box containing six embedded pipes that contain reinforced rebar, and above the surface, there is a granite cover. In the first image, the signals were unclear and noisy due to interference from the surrounding environment. The enhanced image has been

Fig. 6 Enhanced signal processing for GPR scanning: (a) original image; (b) signal processed image.

included in the training data set to increase the variety of training data.

3.3.3 Leveraging image processing

For the GPR data to increase the quality of the output, it needs to adopt image processing techniques. The method utilized uses nonlinear stretching techniques, which enhance the contrast of the image and expand the range of pixel values. Image contrast modification and color adjustment are considered useful methods for increasing the quality of data, thereby enhancing model robustness [58]. The utilized method consists of two stages: first, applying histogram equalization, which involves equalizing a picture's histogram by redistributing all pixel values in the image to achieve an equal number of pixels in each specified output grayscale class; this increases the peak brightness values in the histogram, representing the most populated range. Second, apply adaptive histogram equalization, a local procedure that divides an image into rectangular domains, calculates a histogram for each domain, and adjusts levels to maintain consistency across boundaries, based on the image's nonuniformity and interpolation of intensities [45]. The enhanced contrast from both techniques makes the GPR hyperbola clearer and easier to detect, as shown in Fig. 7.

3.3.4 Data augmentation

Data augmentation is a common approach used to improve model performance. Additionally, it helps prevent overfitting by exposing the model to a wider range of scenarios and variations in the data [59]. To achieve these targets, different techniques are utilized for GPR collected data set, including both signal processing and image processing techniques. These techniques help to create a more diverse and comprehensive data set for training the object detection model. By exposing the model to a wider range of variations, it can learn to better adapt to different scenarios and improve its accuracy in detecting objects in real-world environments. Table 1 lists the data set structure, which consists of two categories: pure data and enhanced data. Pure data refers to images generated directly from GPR scans using an automated conversion method. On the other hand, enhanced data consists of images that have been processed with image and signal processing techniques to improve the visibility of hyperbolas. This enhancement aims to increase the number of trained images and balance the data set by ensuring equal representation of each rebar diameter. This, in turn, leads to more accurate model training.

3.4 Steel rebar detection model

3.4.1 Data labeling and splitting

Data labeling for object detection models is an essential

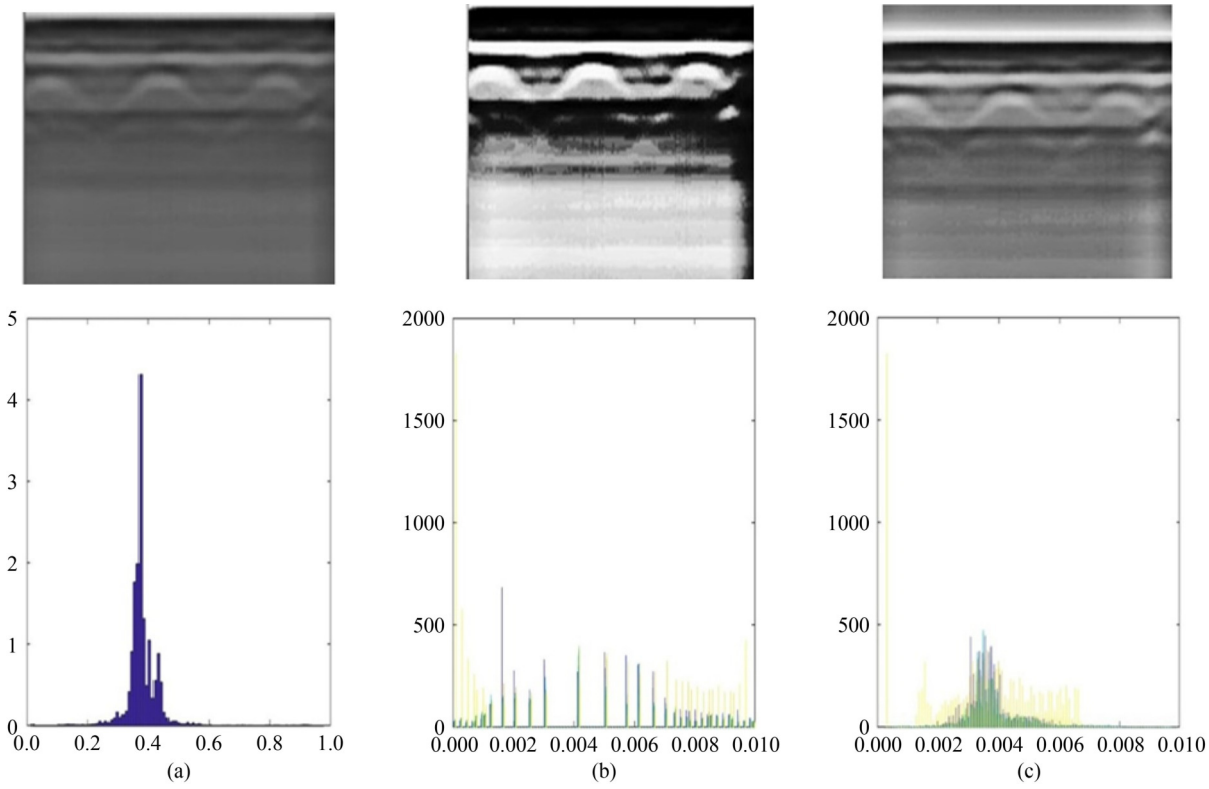

Fig. 7 Enhancement of GPR image using histogram techniques: (a) original image; (b) applying histogram equalization; (c) applying adoptive histogram equalization.

Table 1 Data set structure for the three groups

Group	Rebar diameters	Pure data	Enhanced data
Group 1	Ø16	287	287
	Ø18		
	Ø20		
Group 2	Ø12	141	182
	Ø16		
	Ø20		
Group 3	Ø12	384	938
	Ø16		
	Ø20		

step in training the model to accurately identify and locate objects within an image. The accurate labels are essential for conducting supervised machine learning because the model's performance during operations is directly impacted by the quality of the training data label [60]. Data labeling for the GPR data set was mainly performed by selecting each hyperbola and assigning it to the corresponding rebar diameter. Data splitting is a common technique in machine learning to divide data into a training, testing, or validation set. In this paper, the splitting percentage utilized was 70% of the data for training, 20% for validation, and 10% for testing. Optimal outcomes are achieved by allocating 20%–30% of the data for testing and validation, and the rest (70%–80%) for training. The increasing number of training data points leads to more precise estimations [61]. Additionally, the test set is essential for providing an unbiased evaluation of the model's performance on unseen data, helping to determine its real-world effectiveness [62]. The data set is shuffled first before applying the splitting ratio, which ensures that the model is trained on a diverse set of examples. This helps prevent the model from memorizing patterns specific to the order of images in the data set. This leads to better generalization performance. The number of test images will be increased in future iterations of the model to evaluate its performance across a wider range of scenarios. This will ensure model reliability in real-world applications and utilize the transfer learning concept when training the model on new rebar diameter classes.

3.4.2 Model selection

To determine the best prediction for the GPR-prepared data, a deep model comparison is conducted on a subset of the GPR image data set, in order to utilize the optimal object detection model for detecting rebars and classifying each type through GPR images. Object detection models fall into two main categories: two-stage detector models and one-stage detector models. The two-stage detector models first create a limited number of possible item boxes, which are then categorized and

adjusted. On the other hand, the one-stage detector models identify objects by performing comprehensive and uniform sampling across different locations, sizes, and aspect ratios. The main advantage of the latter lies in its outstanding computational efficiency [63]. This research compares the Faster Region Convolutional Neural Network (R-CNN) model from the two-stage category and YOLO v7 and YOLO v8 from the one-stage category. The selection process is depicted in Fig. 8. All models were trained using the Google Colab cloud service [64], which offers high computational power and easy access to Graphics Processing Units (GPUs) for accelerated training. The Colab service utilized for training includes the T4 GPU and 12 GB of Random Access Memory. The use of cloud computing provides several benefits for training deep learning models, including reduced training time and cost savings compared to on-premise hardware. Additionally, it enables easy scalability and flexibility.

In the first phase, a Faster R-CNN model, which builds upon the R-CNN architecture, is utilized to extract approximately two thousand region proposals from the input image using a selective search algorithm. These region proposals are then passed through a Convolutional Neural Network (CNN) to extract features before being classified into different classes. Then, it utilizes a massive CNN to calculate features for each proposal. Finally, it uses class specific linear Support Vector Machines to classify each region [65]. The faster R-CNN model was developed to address the speed issues of R-CNN by introducing a Region Proposal Network. The model takes an input image, and numerous RoIs are fed into a fully convolutional network. Each RoI is transformed into a feature map of a specific size and then converted into a feature vector using fully connected layers. The network includes two output vectors for each, softmax probabilities, and bounding-box regression offsets specific to each class. The architecture is trained comprehensively with a multi-task loss function [66]. The pre-trained model Faster R-CNN is applied using Detectron2 framework [67]. The benefits of using a pre-trained foundation model include saving time and resources on training a model from scratch, as well as leveraging the knowledge and advancements made by the previous developers of Detectron2. Additionally, using a pre-trained foundation model can lead to improved accuracy and performance in object detection tasks.

In the second phase, YOLO v7 Model is selected. The model consists of four stages, The first stage is the backbone, which serves as the fundamental basis of the model architecture. It is a deep CNN that extracts features from the input image. CNNs can extract complex and abstract properties from input images, recording characteristics across different dimensions and degrees of variation. This allows for more accurate detection and classification of objects, making the backbone stage essential for the overall performance of the model. The second stage is the neck module, which enhances and integrates characteristics acquired from the backbone network at various levels of detail. The third stage is the detection heads, which are responsible for predicting different characteristics of the detected objects using the features they receive from the feature pyramid. Multiple detecting heads are used at different scales and spatial resolutions to effectively handle objects of different sizes. The final stage is bounding box prediction. The prediction head for bounding boxes accurately predicts the precise spatial coordinates of each identified object. Then, the class probability detection head assigns a specific class label to each detected object, indicating it as an individual instance. It quantifies the likelihood that each identified object belongs to a particular class [68]. This allows for accurate and efficient object detection in images with varying scales and sizes. By combining both bounding box prediction and class probability detection, the model can accurately identify and classify objects in complex scenes. The main advantage of utilizing the YOLO v7 model is that it contains a few hyperparameters to tune, making it easier to optimize and faster to train compared to other object detection models. It is important to consider the various parameters that can impact the output of a deep learning model, including layer count, kernel size, optimizers, filters, and batch sizes [69].

In the third phase, the YOLO v8 Model is selected, which improves upon the architecture of the YOLO v7 model, resulting in enhanced speed and accuracy.

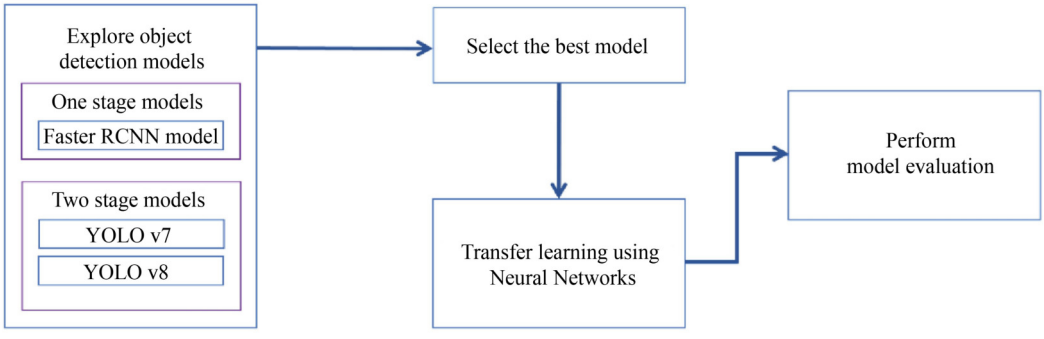

Fig. 8 The object detection model selection process.

Furthermore, it features a revolutionary Path Aggregation Network to enhance the transmission of features and increase context awareness. Utilization of the YOLO v8 model enables enhanced performance and more accurate object recognition in different computer vision applications. Moreover, it incorporates several prediction heads at different scales, resulting in improved detection of objects of diverse sizes. This implementation also presents a customized backbone that incorporates densely coupled convolutions to enhance feature extraction and improve accuracy [70]. YOLO v8's architecture divided the image into a grid of cells. Every single cell makes predictions about bounding boxes and probabilities of different classes. This grid approach enables the model to effectively detect objects at various positions and sizes within the image. The model reaches its velocity and efficiency by directly producing bounding boxes and class probabilities at the granularity of individual grid cells. This grid-based approach allows for the efficient processing of the entire image, eliminating the need for sliding windows or regional proposals. It directly predicts bounding boxes and class probabilities, which streamlines the object detection process and minimizes the use of computational resources [71].

3.4.3 Models evaluation

The performance of the object detection model is evaluated using the Average Precision (AP) metric. The AP metric is a widely used metric for object detection tasks. This metric is dependent on the model's classification outcomes [72]. It utilizes precision−recall metrics, accommodates numerous object categories, and creates a positive prediction by leveraging Intersection over Union (IoU). The factors that affect AP metric are precision, which determines the accuracy of the model's positive predictions by calculating the ratio of true positive predictions to the total number of positive predictions made. Recall, on the other hand, measures the accuracy of a model in properly identifying actual positive cases by calculating the ratio of true positive predictions to the total number of actual positive cases. Second, to manage multiple types of objects, object detection models are required to accurately recognize and determine the precise location of several categories of objects inside an image. The AP metric addresses this issue by determining the mean accuracy (mAP) for each category separately and then averaging these (mAP) values across all categories [73]. Overall, this metric provides a thorough assessment of the model's capabilities [74].

Figure 9 illustrates the process of determining IoU for a GPR image. First, the area of overlap is determined to calculate the intersection of the detected box for predicting reinforcement rebar hyperbola and the ground truth bounding box, which refers to the rebar hyperbola, Then, the union is calculated by adding the areas of both boxes. Finally, the intersection is divided by the union to obtain the IoU value. The IoU ranges from 0 to 1, with higher values indicating better overlap between the detected and ground truth bounding boxes. Moreover, it provides a quantitative measure of how well an algorithm is performing in terms of localization accuracy. Table 2 shows the evaluation results of Faster RCNN, YOLO v7, and YOLO v8 models in terms of mAP at a 0.5 IoU threshold.

3.4.4 Model deployment

After comparing three models, Faster RCNN, YOLO v7, and YOLO v8, it is concluded that the YOLO v8 model provides the highest accuracy. As such, YOLO v8. This model is chosen to train the entire data set, which consists of three classes of rebar diameter Ø12, Ø16, and Ø20.The trained data set consists of 812 images and 1407 enhanced images. The increase in the number of images through data augmentation allows for a more robust training process, resulting in improved accuracy and performance of the YOLO v8 model. This comprehensive data set enables more accurate detection and classification

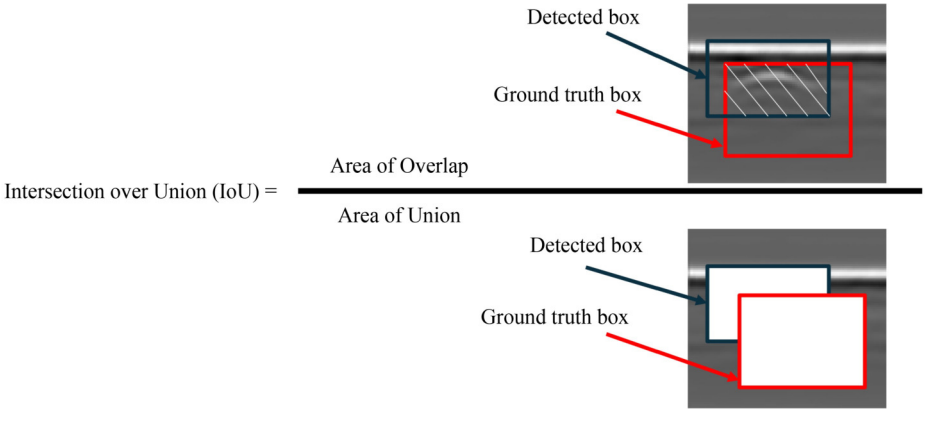

Fig. 9 Illustration of IoU.

of the three classes. Additionally, the increased data set size helps prevent overfitting and ensures better generalization of the model to new data. The data set is split into 70% for training, 20% for validation, and 10% for testing. This division ensures that the model is trained on a diverse range of data and is able to generalize well to unseen examples. The model was trained for 100 epochs. This gave the model sufficient time to learn complex patterns and improve its performance. The model achieves an overall accuracy of 96.6% for the three classes. The accuracy values for rebar diameters Ø12, Ø16, and Ø20 are 97.9%, 94.9%, and 97%, respectively. Figure 10 provides examples of detected and classified images for each class with the detected box colored according to the class. Additionally, the percentage of pixels correctly classified for each diameter is shown.

3.4.5 Transfer learning application on case study

Transfer learning has been extensively utilized in object detection. It involves utilizing the network weights obtained during training on a large and well-labeled data set. These weights are then adjusted, or fine-tuned, for the specific target domain [75]. Using transfer learning provides numerous benefits, including addressing the issue of limited data availability and eliminating the necessity of constructing models from scratch. This can save both time and computational resources. Furthermore, it can improve feature extraction for the new target by leveraging the benefits of previous training on the data set. Using pre-trained models, transfer learning can also lead to improved accuracy and faster convergence during training on smaller data sets. By utilizing transfer learning, the suggested approach not only achieves greater computational efficiency but also outperforms traditional methods in accuracy [4]. During the first trial, the deep model was trained and succeeded in predicting and classifying between three rebar diameters, Ø12, Ø16, and Ø20. One of the most commonly used reinforcement rebars in the Egyptian market is Ø18. Therefore, new data was collected specifically for this diameter from a residential building. The deep model was then fine-tuned using this new data to improve its accuracy in predicting and classifying new rebar diameter. The fine-tuning process involves adjusting the weights of the pre-trained model to better fit the characteristics of the new data, resulting in more precise predictions for this specific diameter.

The newly collected data for the rebar was transformed into images using the developed Python script, described previously. The total number of images obtained is 197. To enhance image clarity and increase the data set size, the same image processing techniques were applied to the entire data set. This approach aims to provide more diverse training data, improve the robustness of the model, and ensure better generalization to new, unseen data. The new number of enhanced images obtained is 197, bringing the total number of images to 304. The new data entered the Robflow cloud service for labeling the data and creating a labeled data set for training the YOLO v8 model. Then, the entire data set was used to train on the YOLO v8 model using the same work flow mention previously, leveraging the benefits of the previous training process. This streamlined process allows for efficient data labeling and model development, ultimately improving the accuracy and performance of the rebar detection system.

Table 2 mAP 50 for Faster RCNN, YOLO v7, and YOLO v8

Class	Faster RCNN	YOLO v7	YOLO v8
All	43.86%	41.90%	99.40%
Ø16	47.29%	53.10%	99.50%
Ø18	45.35%	36.80%	99.20%
Ø20	38.94%	35.80%	99.50%

4 Results and discussions

The previous model weights for YOLO v8 are trained again for 85 epochs with the addition of a new rebar diameter, Ø18. The model is trained for four classes that represented rebar diameters Ø12, Ø16, Ø18, and Ø20. It accurately detects rebar and performs robustly across various hyperbola diameters, ensuring suitability for real-world applications. The model is able to detect Ø12 with an accuracy of 97%, Ø16 with an accuracy of 95.6%,

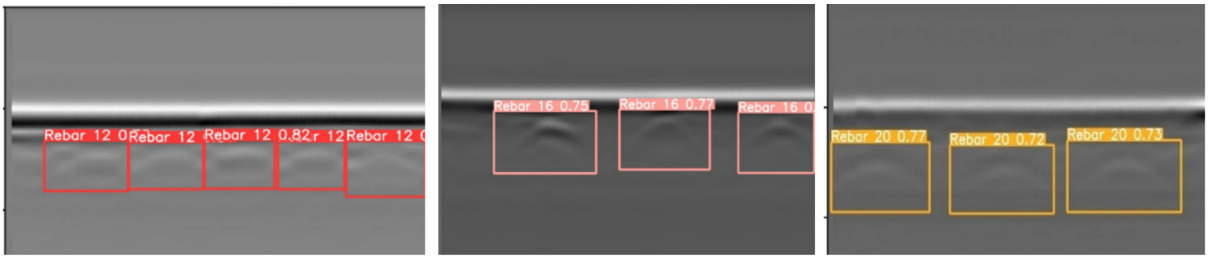

(a) (b) (c)

Fig. 10 Final results for classified and detected rebar: (a) rebar Ø12; (b) rebar Ø16; (c) rebar Ø20.

Ø18 with an accuracy of 98.4%, and Ø20 with an accuracy of 97.9%. The overall accuracy for the four classes is 97.2%. Table 3 lists the model's final mAP 50 score. These results demonstrate the model's effectiveness in accurately identifying different reinforcement rebar sizes. The high accuracy rates across various diameters further validate the model's reliability for practical use in construction projects. To ensure the accuracy of the results, the model is trained three additional times to further improve its performance and robustness in detecting rebar of different sizes in real-world scenarios. The training used the same hyperparameters and configuration as the first time, with the addition of 85 epochs for the second training, 51 epochs for the third, and 51 epochs for the fourth.

Table 3 mAP 50 score for rebar detection

Classes	mAP50
All	97.20%
Ø12	97.00%
Ø16	95.60%
Ø18	98.40%
Ø20	97.90%

Table 4 demonstrates the four training sessions and the corresponding accuracy. It provides 97.2% for the first training, 97.4% for the second, 97.6% for the third, and 97.6% for the fourth. The consistent increase in accuracy with each training iteration demonstrates the model's effectiveness in detecting rebar under various conditions. This validation process ensures the model's reliability and robustness for practical use.

Table 4 Epoch numbers and final results

No. of epochs	Number of epochs	Accuracy (mAP50)
Train 1	85	97.20%
Train 2	50 + 85 = 135	97.40%
Train 3	175 + 51 = 226	97.60%
Train 4	175 + 51 = 226	97.60%

To ensure the model's robustness, several metrics will be presented, including the recall−confidence curve, which illustrates the relationship between recall and confidence level [76]. The recall metric indicates the proportion of actual positive instances correctly detected by the model [77], while the confidence level is a predetermined score that determines whether a prediction should be considered valid. Figure 11 shows the Recall−Confidence curve for the first model training, which demonstrates the relationship between recall and confidence levels for Ø12, Ø16, Ø18, and Ø20 and all classes combined. The curve highlights that as the confidence level increases, recall decreases. This behavior indicates the trade-off between higher confidence predictions and capturing more positive instances. showcasing the model's robustness across all categories.

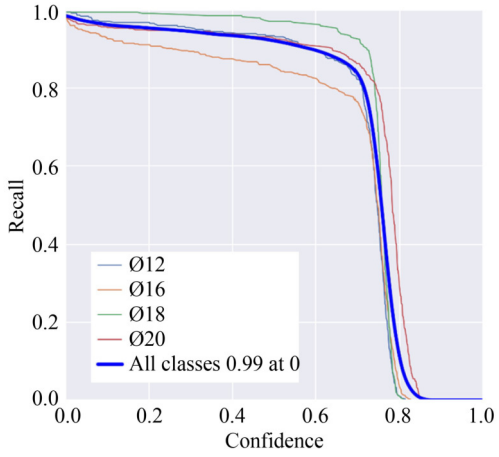

Fig. 11 Recall−confidence curve for rebar classes.

Another important evaluation method is the precision–recall curve, which illustrates the model's resilience and reliability under varied confidence thresholds. These curves evaluate a model's performance by showing the trade-off between precision and recall across different thresholds [76]. Figure 12 presents the results of the first model training, displaying the curves for Ø12, Ø16, Ø18, and Ø20 along with the overall mean Average Precision of 0.972. This result highlights the model's high accuracy in detecting these classes. To further assess the model's effectiveness, the F1 score is utilized. This metric combines precision and recall into a single score, providing a balanced measure of the model's accuracy [78]. Figure 13 displays the F1 scores for the Rebar classes from the first training.

Table 5 lists a comparison of related work using deep models for the localization and classification of reinforced rebar. First, Park et al. [38] utilized the YOLO v3 model for detecting rebar diameter. The model was trained on experimental data. The results demonstrated the importance of considering surrounding environmental factors in rebar detection. In addition, the training process demonstrated the effectiveness of the chosen hyperparameters and activation function in optimizing the model's performance. Second, Xiong and Tan [31] compared different YOLO models to check their performance on field data, finding that YOLO-V4 achieved higher levels of accuracy, recall, F1-score, and mean average precision on site data. Third, Liu et al. [8] trained a SSD model to detect hyperbolas in the GPR image and identify specific RoI. The SSD model can accurately detect hyperbolas, even in noisy or cluttered images. Subsequently, binarization is employed to convert the migrated GPR data into a binary image. This

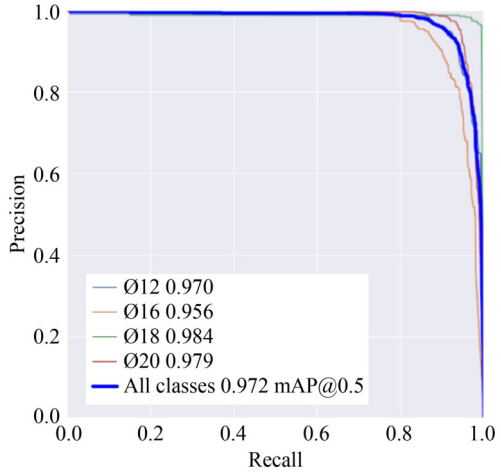

Fig. 12 Precision–recall curve for rebar classes.

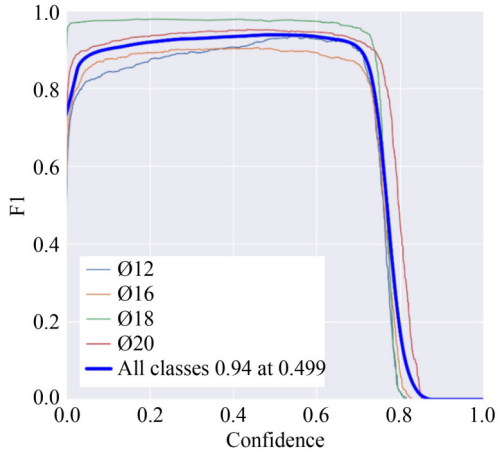

Fig. 13 F1−confidence curve for rebar classes.

Table 5 Model comparison

Ref.	Utilized model	Data set type	mAP
[38]	YOLO v3	Experimental data	93.89%
[31]	YOLO-V4	Field data	99%
[8]	SSD	Field and experimental data	90.90%
[79]	YOLO v3	Field and experimental data	94.80%

involves thresholding the data to retain only the pixels with the highest values. The resulting binary image highlights the rebar response. Finally, apex localization is used to determine the apex of the bright cluster in the binarized image. The apex of the hyperbola is the point where the two branches intersect. This apex information is then used to estimate the horizontal position and depth of the rebar. Testing demonstrated that the suggested system has a detection accuracy of 90.9%. Fourth, Li et al. [79] compared the YOLO v3 model to the Single Shot Multi box Detector and found that YOLO v3 achieved higher precision, recall, and F1-score. In addition, they created concrete specimens to validate the model results. An investigation using these concrete specimens found that 17 of the 22 estimated values (including reinforcing bar diameter and cover thickness) were successfully estimated, while the remaining values had an inaccuracy of up to 2 mm. These experiments demonstrate that the proposed method accurately evaluates reinforcing bar diameter and cover thickness.

From the previous study, it has been noticed that the new model architectures achieved high accuracy in detecting complicated tasks. The improvements in the YOLO models' backbone architectures with each update have enhanced both speed and performance. This balance is essential to the YOLO framework, enabling real-time object detection across several applications [80]. This paper presents the YOLO v8 model, which demonstrates cutting-edge techniques. It enhances object detection accuracy and speed while reducing computational and memory demands. Techniques include attention modules, self-attention mechanisms, spatial pyramid pooling, and deformable convolutions [81]. The YOLO v8 achieved a high mAP of 97.60% when trained on experimental data and then tested on real-world site data. Transfer learning can further improve the model's robustness when trained on new data, leading to enhanced performance in various real-world scenarios.

5 Conclusions

Building assessment is considered an essential step in evaluating the safety and efficiency of buildings. One of the main factors that are considered in the building assessment process is validating the rebar diameter since the reinforced steel has a great impact on the structural integrity of the building. This involves conducting thorough inspections of the rebars to ensure they meet the necessary standards for strength and durability. Additionally, the rebar diameter also plays a crucial role in determining the load-bearing capacity of the building as well as its ability to withstand external forces such as earthquakes or strong winds. It is essential to accurately detect and validate the rebars to prevent any potential structural failures or collapses of the building. Utilizing GPR for the assessment of rebar diameter is a highly effective method, as it is considered a non-destructive testing that can accurately determine the size and condition of the rebars within the concrete structure. Furthermore, integrating AI with GPR technology can enhance the accuracy and efficiency of rebar detection and analysis, providing more detailed insights into the structural integrity of the building. This combination of technologies can help engineers make informed decisions regarding maintenance and repairs to ensure the safety and longevity of the structure.

The paper proposes a framework that consists of four

main stages: 1) data sets creation; 2) data sets processing; 3) steel rebar detection model; 4) transfer learning application on case study. The framework mainly relied on data from both experimental and actual site data to validate the results. The data was converted into images by an automated method, which was developed using Python and R programming languages. Data augmentation methods were utilized to enhance the data set and improve the accuracy of the model using image processing and signal processing techniques. The processed data was then fed into the deep learning model, which was trained to recognize patterns in the images. The results of the model evaluation showed a high level of accuracy using the YOLO v8 model, with an overall accuracy rate of 97%. The model was able to accurately detect and classify various types of rebar. Further, the model was trained four times to further improve its performance and accuracy. The trained model was also tested on unseen data to ensure its generalization capability.

The results demonstrate the efficiency of the trained model, which can be applied to various construction applications. However, challenges such as significant noise interference (e.g., electromagnetic interference generated by the operation of equipment on construction sites), densely distributed steel bars (e.g., in critical parts of large-scale building structures like beams, columns, and slabs), and complex concrete structures (e.g., multi-layered steel bars or irregular shapes in non-standard architectural designs) must be considered. These factors can impact the model's accuracy and the reliability of its predictions, highlighting the need for ongoing refinement and adaptation to real-world conditions. Additionally, the presence of moisture or chloride effects on steel bars can distort GPR waves, further complicating detection. Furthermore, the effect of steel rebar on several concrete structures, such as precast concrete elements, needs to be considered to determine the impact of GPR waves on these elements. These factors highlight the need for further investigation and refinement in future work to enhance the model's performance under real-world construction conditions. This research can be extended in the future by considering using a diverse range of GPR data sets from different sources and different concrete casting techniques (Precast and Cast-*in situ*). Additionally, the performance of the proposed model can be compared with other emerging deep learning models.

Competing interests The authors declare that they have no competing interests.

References

1. Taheri S. A review on five key sensors for monitoring of concrete structures. Construction and Building Materials, 2019, 204: 492–509
2. Zhou F, Chen Z, Liu H, Cui J, Spencer B F, Fang G. Simultaneous estimation of rebar diameter and cover thickness by a GPR-EMI dual sensor. Sensors, 2018, 18(9): 2969
3. Rabczuk T, Belytschko T. Cracking particles: A simplified meshfree method for arbitrary evolving cracks. International Journal for Numerical Methods in Engineering, 2004, 61(13): 2316–2343
4. Goswami S, Anitescu C, Chakraborty S, Rabczuk T. Transfer learning enhanced physics informed neural network for phase-field modeling of fracture. Theoretical and Applied Fracture Mechanics, 2020, 106: 102447
5. Rabczuk T, Belytschko T. A three-dimensional large deformation meshfree method for arbitrary evolving cracks. Computer Methods in Applied Mechanics and Engineering, 2007, 196(29–30): 2777–2799
6. Rabczuk T, Zi G, Bordas S, Nguyen-Xuan H. A simple and robust three-dimensional cracking-particle method without enrichment. Computer Methods in Applied Mechanics and Engineering, 2010, 199(37–40): 2437–2455
7. Tosti F, Ferrante C. Using ground penetrating radar methods to investigate reinforced concrete structures. Surveys in Geophysics, 2020, 41(3): 485–530
8. Liu H, Lin C, Cui J, Fan L, Xie X, Spencer B F. Detection and localization of rebar in concrete by deep learning using ground penetrating radar. Automation in Construction, 2020, 118: 103279
9. Oikonomopoulou E C, Palieraki V A, Sfikas I P, Trezos C G. Reliability and limitations of GPR for identifying objects embedded in concrete—Experience from the lab. Case Studies in Construction Materials, 2022, 16: e00898
10. Dou Q, Wei L, Magee D R, Cohn A G. Real-time hyperbola recognition and fitting in GPR data. IEEE Transactions on Geoscience and Remote Sensing, 2017, 55(1): 51–62
11. Küçükdemirci M, Sarris A. GPR data processing and interpretation based on artificial intelligence approaches: Future perspectives for archaeological prospection. Remote Sensing, 2022, 14(14): 3377
12. Liu G, Gao W, Liu W, Chen Y, Wang T, Xie Y, Bai W, Li Z. Automatic defect classification for infrared thermography in CFRP based on deep learning dense convolutional neural network. Journal of Nondestructive Evaluation, 2024, 43(3): 73
13. Huangfu Z, Li S. Lightweight You Only Look Once v8: An upgraded You Only Look Once v8 algorithm for small object identification in unmanned aerial vehicle images. Applied Sciences, 2023, 13(22): 12369
14. He C, Saha P. Investigating YOLO models towards outdoor obstacle detection for visually impaired people. 2023, arXiv:2312.07571
15. Faris N, Zayed T, Abdelkader E M, Fares A. Corrosion assessment using ground penetrating radar in reinforced concrete structures: Influential factors and analysis methods. Automation in Construction, 2023, 156: 105130
16. Zhang J, Peng L, Wen S, Huang S. A review on concrete structural properties and damage evolution monitoring techniques. Sensors, 2024, 24(2): 620
17. Wang B, Zhong S, Lee T L, Fancey K S, Mi J. Non-destructive testing and evaluation of composite materials/structures: A state-

of-the-art review. Advances in Mechanical Engineering, 2020, 12(4): 1–28
18. Verma S K, Bhadauria S S, Akhtar S. *In-situ* condition monitoring of reinforced concrete structures. Frontiers of Structural and Civil Engineering, 2016, 10(4): 420–437
19. Yue Y, Liu H, Lin C, Meng X, Liu C, Zhang X, Cui J, Du Y. Automatic recognition of defects behind railway tunnel linings in GPR images using transfer learning. Measurement, 2024, 224: 113903
20. Gao Z, Fu Z, Wen M, Guo Y, Zhang Y. Physical informed neural network for thermo-hydral analysis of fire-loaded concrete. Engineering Analysis with Boundary Elements, 2024, 158: 252–261
21. Spears M, Hedjazi S, Taheri H. Ground penetrating radar applications and implementations in civil construction. Journal of Structural Integrity and Maintenance, 2023, 8(1): 36–49
22. Wang, X, Zhang, Y, Liu, Q, Wang, H. Prediction of the pore-pressure built-up and temperature of fire-loaded concrete with Pix2Pix. Computers, Materials and Continua, 2024, 79(2): 2907–2922
23. Dinh K, Gucunski N, Kim J, Duong T H. Understanding depth-amplitude effects in assessment of GPR data from concrete bridge decks. NDT and E International, 2016, 83: 48–58
24. Tesic K, Baricevic A, Serdar M, Gucunski N. Characterization of ground penetrating radar signal during simulated corrosion of concrete reinforcement. Automation in Construction, 2022, 143: 104548
25. Hong S, Chen D, Dong B. Numerical simulation and mechanism analysis of GPR-based reinforcement corrosion detection. Construction and Building Materials, 2022, 317: 125913
26. Rhee J Y, Shim J, Kee S H, Lee S Y. Different characteristics of radar signal attenuation depending on concrete condition of bare bridge deck. KSCE Journal of Civil Engineering, 2020, 24(7): 2049–2062
27. Lachowicz J, Rucka M. A novel heterogeneous model of concrete for numerical modelling of ground penetrating radar. Construction and Building Materials, 2019, 227: 116703
28. Asadi P, Gindy M, Alvarez M. A machine learning based approach for automatic rebar detection and quantification of deterioration in concrete bridge deck ground penetrating radar B-scan images. KSCE Journal of Civil Engineering, 2019, 23(6): 2618–2627
29. Kaur P, Dana K J, Romero F A, Gucunski N. Automated GPR rebar analysis for robotic bridge deck evaluation. IEEE Transactions on Cybernetics, 2016, 46(10): 2265–2276
30. Ahmed H, Le C P, La H M. Pixel-level classification for bridge deck rebar detection and localization using multi-stage deep encoder–decoder network. Developments in the Built Environment, 2023, 14: 100132
31. Xiong X, Tan Y. Deep learning-based detection of tie bars in concrete pavement using ground penetrating radar. International Journal of Pavement Engineering, 2023, 24(2): 2155648
32. Chang C W, Lin C H, Lien H S. Measurement radius of reinforcing steel bar in concrete using digital image GPR. Construction and Building Materials, 2009, 23(2): 1057–1063
33. Giannakis I, Giannopoulos A, Warren C. A machine learning scheme for estimating the diameter of reinforcing bars using ground penetrating radar. IEEE Geoscience and Remote Sensing Letters, 2021, 18(3): 461–465
34. Zhang Y, Gao Z, Wang X, Liu Q. Image representations of numerical simulations for training neural networks. Computer Modeling in Engineering & Sciences, 2023, 134(2): 821–833
35. Xiang Z, Ou G, Rashidi A. An innovative approach to determine rebar depth and size by comparing GPR data with a theoretical database. In: Construction Research Congress 2020. Reston, VA: American Society of Civil Engineers, 2020, 86–95
36. Zhuang X, Guo H, Alajlan N, Zhu H, Rabczuk T. Deep autoencoder based energy method for the bending, vibration, and buckling analysis of Kirchhoff plates with transfer learning. European Journal of Mechanics. A, Solids, 2021, 87: 104225
37. Liu F, Liu J, Wang L. Deep learning and infrared thermography for asphalt pavement crack severity classification. Automation in Construction, 2022, 140: 104383
38. Park S, Kim J, Jeon K, Kim J, Park S. Improvement of gpr-based rebar diameter estimation using YOLO-v3. Remote Sensing, 2021, 13(10): 2011
39. Kuchipudi S T, Ghosh D, Gupta H. Automated assessment of reinforced concrete elements using ground penetrating radar. Automation in Construction, 2022, 140: 104378
40. Xue C, Xia Y, Wu M, Chen Z, Cheng F, Yun L. EL-YOLO: An efficient and lightweight low-altitude aerial objects detector for onboard applications. Expert Systems with Applications, 2024, 256: 124848
41. Lin H, Parsi A, Mullins D, Horgan J, Ward E, Eising C, Denny P, Deegan B, Glavin M, Jones E. A study on data selection for object detection in various lighting conditions for autonomous vehicles. Journal of Imaging, 2024, 10(7): 153
42. Li L, Yang L, Hao Z, Sun X, Chen G. Road sub-surface defect detection based on gprMax forward simulation-sample generation and Swin Transformer-YOLOX. Frontiers of Structural and Civil Engineering, 2024, 18(3): 334–349
43. Alzubi J, Nayyar A, Kumar A. Machine learning from theory to algorithms: An overview. Journal of Physics: Conference Series, 2018, 1142: 012012
44. Liao L, Li H, Shang W, Ma L. An empirical study of the impact of hyperparameter tuning and model optimization on the performance properties of deep neural networks. ACM Transactions on Software Engineering and Methodology, 2022, 31(3): 1–40
45. Li J, Cheng K, Wang S, Morstatter F, Trevino R P, Tang J, Liu H. Feature selection: A data perspective. ACM Computing Surveys, 2017, 50(6): 1–45
46. Mumuni A, Mumuni F. Data augmentation: A comprehensive survey of modern approaches. Array, 2022, 16: 100258
47. Raschka S. Model evaluation, model selection, and algorithm selection in machine learning. 2018, arXiv:1811.12808
48. Singh V, Pencina M, Einstein A J, Liang J X, Berman D S, Slomka P. Impact of train/test sample regimen on performance estimate stability of machine learning in cardiovascular imaging. Scientific Reports, 2021, 11(1): 14490
49. Zhuang F, Qi Z, Duan K, Xi D, Zhu Y, Zhu H, Xiong H, He Q. A comprehensive survey on transfer learning. Proceedings of the IEEE, 2021, 109(1): 43–76
50. Manataki M, Vafidis A, Sarris A. GPR data interpretation

approaches in archaeological prospection. Applied Sciences, 2021, 11(16): 7531
51. Gautier L. rpy2. 2024 (available at the website of GitHub)
52. Harris C R, Millman K J, Van Der Walt S J, Gommers R, Virtanen P, Cournapeau D, Wieser E, Taylor J, Berg S, Smith N J, et al. Array programming with NumPy. Nature, 2020, 585(7825): 357–362
53. Hunter, J. D. Matplotlib: A 2D graphics environment. Computing in Science and Engineering, 2007, 9(3): 90–95
54. Bianchini Ciampoli L, Tosti F, Economou N, Benedetto F. Signal processing of GPR data for road surveys. Geosciences, 2019, 9(2): 96
55. Benedetto A, Tosti F, Bianchini Ciampoli L, D'Amico F. An overview of ground-penetrating radar signal processing techniques for road inspections. Signal Processing, 2017, 132: 201–209
56. Ardeti V A, Kolluru V R, Varghese G T, Patjoshi R K. An overview on state-of-the-art electrocardiogram signal processing methods: Traditional to AI-based approaches. Expert Systems with Applications, 2023, 217: 119561
57. Maruddani B, Sandi E. The development of ground penetrating radar (GPR) data processing. International Journal of Machine Learning and Computing, 2019, 9(6): 768–773
58. Yang C C. Image enhancement by modified contrast-stretching manipulation. Optics and Laser Technology, 2006, 38(3): 196–201
59. Lashgari E, Liang D, Maoz U. Data augmentation for deep-learning-based electroencephalography. Journal of Neuroscience Methods, 2020, 346: 108885
60. Desmond M, Muller M, Ashktorab Z, Dugan C, Duesterwald E, Brimijoin K, Finegan-Dollak C, Brachman M, Sharma A, Joshi N, et al. Increasing the speed and accuracy of data labeling through an ai assisted interface. In: Proceedings of the 26th International Conference on Intelligent User Interfaces. New York: Association for Computing Machinery, 2021, 392–401
61. Gholamy A, Kreinovich V, Kosheleva O. Why 70/30 or 80/20 relation between training and testing sets: A pedagogical explanation. International Journal of Intelligent Technology and Applications, 2018, 11(2): 105–111
62. Birba D E. A comparative study of data splitting algorithms for machine learning model selection. Thesis for the Master's Degree. Stockholm: KTH Royal Institute of Technology, 2020
63. Li K, Cao L. A review of object detection techniques. In: 2020 5th International Conference on Electromechanical Control Technology and Transportation. Nanchang: IEEE, 2020, 385–390
64. Google Colab. Google Colaboratory. 2025 (available at the website of Colab)
65. Girshick R, Donahue J, Darrell T, Malik J. Rich feature hierarchies for accurate object detection and semantic segmentation. In: Proceedings of the IEEE Conference on Computer Vision and Pattern Recognition. Columbus, OH: IEEE, 2014, 580–587
66. Girshick R. Fast R-CNN. In: Proceedings of the IEEE International Conference on Computer Vision. Santiago: IEEE, 2015, 1440–1448
67. Wu Y, Kirillov A, Massa F, Lo W-Y, Girshick R. Detectron2. 2019 (available at the website of GitHub)
68. Kumar P K, Kumar N K. Drone-based apple detection: Finding the depth of apples using YOLOv7 architecture with multi-head attention mechanism. Smart Agricultural Technology, 2023, 5: 100311
69. El-Maraghy M, Metawie M, Safaan M, Saad Eldin A, Hamdy A, El Sharkawy M, Abdelaty A, Azab S, Marzouk M. Predicting energy consumption of mosque buildings during the operation stage using deep learning approach. Energy and Building, 2024, 303: 113829
70. Elavarasu M, Govindaraju K. Unveiling the advancements: YOLOv7 vs YOLOv8 in pulmonary carcinoma detection. Journal of Robotics and Control, 2024, 5(2): 459–470
71. Padilla R, Netto S L, da Silva E. A. A survey on performance metrics for object-detection algorithms. In: 2020 International Conference on Systems, Signals and Image Processing. Niteroi: IEEE, 2020, 237–242
72. Juan Y, Ke Z, Chen Z, Zhong D, Chen W, Yin L. Rapid density estimation of tiny pests from sticky traps using Qpest RCNN in conjunction with UWB-UAV-based IoT framework. Neural Computing and Applications, 2024, 36(17): 9779–9803
73. Terven J, Cordova-Esparza D. A comprehensive review of YOLO: From YOLOv1 to YOLOv8 and beyond. 2023, arXiv:2304.00501
74. Liu C, Yao Y, Li J, Qian J, Liu L. Research on lightweight GPR road surface disease image recognition and data expansion algorithm based on YOLO and GAN. Case Studies in Construction Materials, 2024, 20: e02779
75. Sahito A, Frank E, Pfahringer B. Transfer of pretrained model weights substantially improves semi-supervised image classification. In AI 2020: Advances in Artificial Intelligence: 33rd Australasian Joint Conference. Canberra, ACT: 2020, 33: 433–444
76. Aktouf L, Shivanna Y, Dhimish M. High-precision defect detection in solar cells using YOLOv10 deep learning model. Solar, 4(4): 2024, 639–659
77. Hicks S A, Strümke I, Thambawita V, Hammou M, Riegler M A, Halvorsen P, Parasa S. On evaluation metrics for medical applications of artificial intelligence. Scientific Reports, 2022, 12(1): 5979
78. Santos C, Aguiar M, Welfer D, Belloni B. A new approach for detecting fundus lesions using image processing and deep neural network architecture based on YOLO model. Sensors, 2022, 22(17): 6441
79. Li X, Liu H, Zhou F, Chen Z, Giannakis I, Slob E. Deep learning-based nondestructive evaluation of reinforcement bars using ground-penetrating radar and electromagnetic induction data. Computer-Aided Civil and Infrastructure Engineering, 2022, 37(14): 1834–1853
80. Safaldin M, Zaghden N, Mejdoub M. An improved YOLOv8 to detect moving Objects. IEEE Access, 2024, 12: 59782–59806
81. Sohan M, Sai Ram T, Reddy R, Venkata C. A review on YOLOv8 and its advancements. In: International Conference on Data Intelligence and Cognitive Informatics. Singapore: Springer, 2024, 529–545